ENCIT 2018

ABCM Associação Brasileira de Engenharia e Ciências Mecânicas

17th Brazilian Congress of Thermal Sciences and Engineering
November 25th-28th, 2018, Águas de Lindóia, SP, Brazil

ENCIT-2018-0045
TRANSIENT NUMERICAL SIMULATION OF A LIQUID-VAPOR MIXTURE WITH INTERPHASE MASS TRANSFER

Bruno Resende Rodrigues
Eugênio Spanó Rosa
University of Campinas, Faculty of Mechanical Engineering, SP, Brazil
brunorodri@fem.unicamp.br

Abstract. *A transient flow simulator for a pure substance in thermal equilibrium with liquid and gas phases using the drift-flux model is developed. An eight-order compact finite difference scheme is used to evaluate the solution numerically with an artificial viscosity term to stabilize the solution close to discontinuities. The model is validated against two tests. The first test consists of a steady state solution from the literature. The flow is adiabatic with constant mixture enthalpy in steady state conditions. The second test uses a two-phase shock tube case found in the literature. The maximum errors were of 6% due to differences on the property evaluation. The present model was also shown to sharply capture discontinuities in the numerical solution and also due to the difference in order of the two numerical schemes.*

Keywords: *drift-flux model, transient simulation, gas-liquid flow, compact scheme, interphase mass transfer*

1. INTRODUCTION

The production of crude petroleum faces a challenge to ensure the successful and economical flow from the reservoir to the oil tank. The motivation of this work is towards flow assurance focusing on the prevention of solid deposits such gas hydrates, asphaltene, wax and naphthenates. The scenarios of occurrence solids formation is likely to happen during the start up of lines. The flow is characterized by a transient regime where a fraction of liquid is transformed into vapor exhibiting a pressure and temperature history which may favor the precipitation of solids. This is a complex phenomenon which involves not only the flow field and the associated thermodynamics properties but also non-equilibrium thermodynamics and chemical kinetics.

This work addresses specifically to the transient flow simulation of a pure fluid with phase change using Drift Flux model. A brief review of works discloses the majority of authors employing the homogenous equilibrium model, HEM, and also the homogeneous relaxation model HRM. Saurel *et al.* (2008) model the cavitating and flashing flows employing a five equation system. The authors claim the conventional Gudonov-type schemes for non-conservative hyperbolic system are not suitable for high resolution. The authors propose a relaxation-projection method extended to the context of the multiphase model. At each time step, the hyperbolic system in absence of heat and mass transfer is solved to provide a non equilibrium hydrodynamic field. The interfacial mass transfer is determined using a relaxation technique proportional to the Gibbs free energy difference between the vapor and the liquid phase. Lund and Aursand (2012) developed a four equation model to simulate the flow of a two phase CO_2 pipeline with phase transfer. The system of equations is solved by the fractional method (Leveque, 2002). The conservative hyperbolic system is solved using the multi-stage MUSTA approach (Toro, 2009). The advantage of MUSTA scheme, compared to other Riemann solvers, is that is relatively simple. The interfacial mass transfer is derived from a relaxation technique which is proportional to the differences of the chemical potential of the vapor and liquid phases. The authors propose an analytical expression, based on the statistical rate theory, instead of using a constant of proportionality based on experimental data. Brown *et al.* (2013) develops a homogeneous relaxation flow model for simulating the rupture of CO_2 pipelines. A system with four equations is solved using the fractional technique. The conservative hyperbolic system is solved using a Gudonov method using HLL Riemann solver (Toro, 2009). The interfacial mass transfer term is determined using the relaxation technique based on Downar-Zapolski *et al.* (1996) but with updated coefficients applied to the CO_2. Lorenzo *et al.* (2017) develops a code for fast transients water-vapor applied to the nuclear industry based on system of four equations. The system of equations is solved using the fractional technique. The conservative hyperbolic system is solved using a Gudonov method using HLLC Riemann solver (Toro, 2009).

This short review shows that the fast transient models for a single component with phase change rely on Gudonov method embodied in several schemes of Riemann solvers. These solvers represent the physics of the flow and the numerical results proved to be accurate. The construction of the fluxes due right and left waves requires the knowledge of the phase sound speed and also the fluid properties such as density and energy. The Riemann solvers have constructed

variables involving the primitive variables, such as velocities, void fraction, quality, densities and energy. The solution of the system has to fulfill the hyperbolic set of equations with properties defined by an Equation of State (EoS). It is not an easy task to find the thermodynamic properties to the solution of the hyperbolic equations.

The objective of this work is to introduce a finite differences compact scheme to solve the system of hyperbolic equations. One of the advantages of this method is the use the conserved variables to match the thermodynamic constraints and the method does not explicitly require the sound speed. The scheme employed in this work is of eighth order of accuracy in space and fourth order in time. The method allows drift between the liquid and vapor and appropriately changing the drift constants it can also represent the Homogeneous Equilibrum Model. Artificial diffusivities are introduced into the system of equations to stabilize the solution close to discontinuities in analogy to a procedure by Cook and Cabot (2004) for the Euler equations. Due to the high order of the method, it is expected that discontinuities present in the numerical solution are sharply captured by the present method.

2. DRIFT-FLUX MODEL

A three equation model for 1D, transient flow of a saturated pure substance with two phases in thermal equilibrium and with interphase mass transfer is presented in Eqs. (1) to (2). The first equation, Eq. (1), corresponds to the mixture mass conservation equation, Eq. (2) is the mixture momentum equation and Eq. (3) is the mixture energy equation.

$$\frac{\partial}{\partial t}[((1-\alpha)\rho_l + \alpha\rho_g)A] + \frac{\partial}{\partial z}[((1-\alpha)\rho_l v_l + \alpha\rho_g v_g)A] = 0\,, \tag{1}$$

$$\frac{\partial}{\partial t}[((1-\alpha)\rho_l v_l + \alpha\rho_g v_g)A] + \frac{\partial}{\partial z}[((1-\alpha)\rho_l v_l^2 + \alpha\rho_g v_g^2 + P)A] = s_m\,, \tag{2}$$

$$\frac{\partial}{\partial t}[((1-\alpha)\rho_l \hat{u}_l + \alpha\rho_g \hat{u}_g)A] + \frac{\partial}{\partial z}[((1-\alpha)\rho_l v_l \hat{u}_l + \alpha\rho_g v_g \hat{u}_g + P((1-\alpha)v_l + \alpha v_g))A] = 0\,. \tag{3}$$

In Eqs. (1) through (3), the subscripts l and g refer to the liquid and gas phases respectively, α is the void fraction, A is the pipe cross sectional area, ρ_k, v_k and $\hat{u}_k$ are the density, velocity and internal energy of each phase. Both phases are assumed to be in thermodynamic equilibrium and share the same pressure p and temperature T, which correspond to the saturation state. The source term s_m present in the momentum equation is defined in Eq. (6). Source terms due to friction or the gravitational force in the energy equation were assumed to be small and, therefore, neglected in the present model. The system of hyperbolic equations can be written in vector form as:

$$\frac{\partial \boldsymbol{Q}}{\partial t} + \frac{\partial \boldsymbol{F}}{\partial x} = \boldsymbol{S}\,, \tag{4}$$

where

$$\begin{aligned} \boldsymbol{Q} &= \begin{bmatrix} q_1 \\ q_2 \\ q_2 \end{bmatrix} = \begin{bmatrix} [(1-\alpha)\rho_l + \alpha\rho_g]A \\ [(1-\alpha)\rho_l v_l + \alpha\rho_g v_g])A \\ [(1-\alpha)\rho_l \hat{u}_l + \alpha\rho_g \hat{u}_g]A \end{bmatrix}\,,\ \boldsymbol{S} = \begin{bmatrix} 0 \\ s_m \\ 0 \end{bmatrix} \text{ and} \\ \boldsymbol{F} &= \begin{bmatrix} f_1 \\ f_2 \\ f_3 \end{bmatrix} = \begin{bmatrix} [(1-\alpha)\rho_l v_l + \alpha\rho_g v_g]A \\ [(1-\alpha)\rho_l v_l^2 + \alpha\rho_g v_g^2 + P]A \\ [(1-\alpha)\rho_l v_l \hat{u}_l + \alpha\rho_g v_g \hat{u}_g + P((1-\alpha)v_l + \alpha v_g)]A \end{bmatrix}\,. \end{aligned} \tag{5}$$

The momentum source term s_m includes both viscous friction inside the duct and gravitational effects see Eq.(6):

$$s_m = -\frac{f j_m |j_m|}{2D}A - [(1-\alpha)\rho_l + \alpha\rho_g]gA\sin(\theta)\,, \tag{6}$$

where D is the pipe diameter and θ is the pipe inclination in relation to a horizontal plane. The mixture velocity j_m is defined in Eq. (7) in terms of the gas and liquid superficial velocities, j_g and j_l:

$$\begin{aligned} j_m &= j_g + j_l\,, \\ j_g &= \alpha v_g\,, \\ j_l &= (1-\alpha)v_l\,. \end{aligned} \tag{7}$$

The friction factor f is a function of the two-phase Reynolds number:

$$Re_m = \frac{\rho_m j_m D}{\mu_m} \, . \tag{8}$$

The mixture viscosity μ_m is defined in Eq. (9) (Beattie and Whalley, 1982), while the mixture density ρ_m is defined in Eq. (10):

$$\mu_m = (1.0 - \alpha)\mu_l(1.0 + 2.5\alpha) + \alpha\mu_g \, , \tag{9}$$

$$\rho_m = \alpha\rho_g + (1 - \alpha)\rho_l \, . \tag{10}$$

For turbulent flows, the implicit Colebrook-White correlation is used:

$$\frac{1}{\sqrt{f}} = -2.0 \log\left(\frac{\epsilon/D}{3.7} + \frac{2.51}{Re_m\sqrt{f}}\right) . \tag{11}$$

Due to the saturated pure substance hypothesis, the densities and internal energies of both phases are functions of only the pressure p. Therefore, the system of equations given by Eq. (4) has four unknowns (α, p, v_l and v_g), but only three equations. The kinematic relation proposed by Zuber and Findlay (1965), shown in Eq. (12), provides an additional equation to close the system:

$$v_g = C_0 j_m + v_d \, , \tag{12}$$

where the distribution parameter C_0 and drift velocity v_d depend on the flow pattern and the fluid transport properties. Note that setting $C_0 = 1.0$ and $v_d = 0.0$ in Eq. (12) implies that $v_g = v_l = v$, which recovers the Homogeneous Equilibrium Model.

3. NUMERICAL MODEL

This model employs a finite differences high-order compact scheme. Given the centered nature of the scheme, spurious oscillations arise near discontinuities. Non-linear artificial diffusivities are introduced to the model to stabilize the solution near shocks. These artificial terms are adapted to the drift-flux model using mixture properties and then validated using two test cases.

3.1 Artificial Diffusivity

An artificial viscous stress term τ_* is introduced into the components of f_2 and f_3 of the flux vector, corresponding to the energy and momentum equations. They are necessary to stabilize the solution near discontinuities, such as shocks. The definition of τ_* is based on the one presented by Cook and Cabot (2004) for the Euler equations. Here, it is defined in terms of the mixture superficial velocity j_m and mixture density ρ_m, as shown in Eqs. (13) and (14):

$$\tau_* = \mu_* \frac{\partial j_m}{\partial z} \, , \tag{13}$$

$$\mu_* = C_\mu \rho_m (\Delta z)^{r+1} \overline{|j_{m,i}^{(r)}|} \, , \tag{14}$$

where μ_* is the artificial viscosity, Δz is the grid spacing, $j_{m,i}^{(r)}$ denotes an r^{th} order derivative of j_m at point i in the grid and C_μ is a calibration constant. In the present work, a fourth derivative was used, $r = 4$, and $C_\mu = 2.5$ was chosen after calibrating the computational model. The fourth order derivative $j_{m,i}^{(iv)}$ was evaluated as shown in Eq. (15):

$$\begin{aligned} \frac{7}{26} j_{m,i-1}^{(iv)} + j_{m,i}^{(iv)} + \frac{7}{26} j_{m,i-1}^{(iv)} \; = \; & \frac{1}{78(\Delta x)^4}(j_{m,i+3} - 9j_{m,i+1} + 16v_i - 9j_{m,i-1} + j_{m,i-3}) + \\ & + \frac{7}{26(\Delta x)^4}(j_{m,i+2} - 4j_{m,i+1} + 6v_i - 4j_{m,i-1} + j_{m,i-2}) \, , \end{aligned} \tag{15}$$

and the operator $\overline{|j_{m,i}^{(iv)}|}$ corresponds to a Gaussian filter (Cook and Cabot, 2004) applied to the absolute value of $j_{m,i}^{(iv)}$, shown in Eq. (16).

$$\begin{aligned}\overline{|j_{m,i}^{(iv)}|} = \frac{3565}{10368}|j_{m,i}^{(iv)}| + \frac{3091}{12960}(|j_{m,i+1}^{(iv)}| + |j_{m,i-1}^{(iv)}|) + \frac{1997}{2592}(|j_{m,i+2}^{(iv)}| + |j_{m,i-2}^{(iv)}|) + \\ + \frac{149}{12960}(|j_{m,i+3}^{(iv)}| + |j_{m,i-3}^{(iv)}|) + \frac{107}{103680}(|j_{m,i+4}^{(iv)}| + |j_{m,i-4}^{(iv)}|)\,.\end{aligned} \tag{16}$$

The artificial stress term τ_* is introduced in the momentum and energy equations, Eqs. (2) and (3). It is defined in terms of the mixture superficial velocity, j_m. The artificial diffusivity τ_* will not detect sharp gradients such as contact discontinuities because it is only linked to the velocities. Another artificial diffusivity χ_* is defined in Eq. (17) to be introduced in the mixture mass equation and dampen oscillations close to contact discontinuities. It is defined in Eq. (17):

$$\chi_* = C_\chi j_m (\Delta z)^{r+1} \overline{|x_i^{(r)}|} \frac{\partial \rho_m}{\partial z}\,, \tag{17}$$

where x is the quality:

$$x = \frac{\dot{m}_v}{\dot{m}_m} = \frac{1}{1 + \frac{\rho_l j_l}{\rho_g j_g}}\,. \tag{18}$$

A fourth derivative was also chosen for the evaluation of χ_*, therefore $r = 4$ in Eq. (17) and the calibration constant C_χ was set as $C_\chi = 2.0$. The fourth derivative and the gaussian filter are evaluated using Eqs. (15) and (16).

With τ_* and χ_* properly defined, the modified flux vector $\boldsymbol{F}^*$ is evaluated as shown in Eq. (19):

$$\boldsymbol{F}^* = \begin{bmatrix} f_1^* \\ f_2^* \\ f_3^* \end{bmatrix} \begin{bmatrix} [(1-\alpha)\rho_l v_l + \alpha\rho_g v_g - \chi_*]A \\ [(1-\alpha)\rho_l v_l^2 + \alpha\rho_g v_g^2 + P - \tau_*]A \\ [(1-\alpha)\rho_l v_l \hat{u}_l + \alpha\rho_g v_g \hat{u}_g + (P-\tau_*)((1-\alpha)v_l + \alpha v_g)]A \end{bmatrix}\,. \tag{19}$$

The system of equations to be solved is then given by Eq. (20):

$$\frac{\partial \boldsymbol{Q}}{\partial t} + \frac{\partial \boldsymbol{F}^*}{\partial z} = \boldsymbol{S}\,, \tag{20}$$

where $\boldsymbol{Q}$ and $\boldsymbol{S}$ are defined in Eq. (5) and $\boldsymbol{F}^*$ is defined in Eq. (19).

3.2 Finite Differences Model

The system of non-linear partial differential equations (PDEs) presented in Eq. (4) was solved numerically. The first step applies a spatial discretization to the $\frac{\partial \boldsymbol{F}^*}{\partial z}$ term, reducing the problem to a system of ordinary differential equations (ODEs) in time. The finite differences method was used to achieve this, using an eight-order compact scheme presented in Eq. (21) (Lele, 1992) to approximate the spatial derivatives:

$$\frac{3}{8}\Big(\frac{\partial f^*}{\partial z}\Big)_{i-1} + \Big(\frac{\partial f^*}{\partial z}\Big)_i + \frac{3}{8}\Big(\frac{\partial f^*}{\partial z}\Big)_{i+1} = \frac{1}{\Delta z}\Big[-\frac{1}{480}(f_{i+3}^* - f_{i-3}^*) + \frac{1}{20}(f_{i+2}^* - f_{i-2}^*) + \frac{25}{32}(f_{i+i}^* - f_{i-i}^*)\Big]\,. \tag{21}$$

In Eq. (21), f^* can represent any of the components f_1^*, f_2^* or f_3^* of the modified flux vector $\boldsymbol{F}^*$ defined in Eq. (19).

A different scheme was used for points near boundary points. For a computational domain with I discreet points with boundaries at $i = 0$ and $i = I - 1$, these near-boundary points are $i = 1$, $i = 2$, $i = I - 3$ and $i = I - 2$. The schemes for these points are shown in Eqs. (22) through (25):

$$\Big(\frac{\partial f^*}{\partial z}\Big)_1 + 2\Big(\frac{\partial f^*}{\partial z}\Big)_2 = \frac{1}{\Delta z}\Big(-\frac{1}{10}f_0^* - \frac{25}{12}f_1^* + \frac{4}{3}f_2^* + 1f_3^* - \frac{1}{6}f_4^* + \frac{1}{60}f_5^*\Big)\,, \tag{22}$$

$$\frac{1}{4}\Big(\frac{\partial f^*}{\partial z}\Big)_1 + \Big(\frac{\partial f^*}{\partial z}\Big)_2 + \frac{1}{2}\Big(\frac{\partial f^*}{\partial z}\Big)_3 = \frac{1}{\Delta z}\Big(-\frac{1}{60}f_0^* - \frac{31}{48}f_1^* - \frac{1}{3}f_2^* + \frac{11}{12}f_3^* + \frac{1}{12}f_4^* - \frac{1}{240}f_5^*\Big)\,, \tag{23}$$

$$\frac{1}{2}\Big(\frac{\partial f^*}{\partial z}\Big)_{I-4}+\Big(\frac{\partial f^*}{\partial z}\Big)_{I-3}+\frac{1}{4}\Big(\frac{\partial f^*}{\partial z}\Big)_{I-2}=\frac{1}{\Delta z}\Big(\frac{1}{240}f^*_{I-6}-\frac{1}{12}f^*_{I-5}-\frac{11}{12}f^*_{I-4}+\frac{1}{3}f^*_{I-3}+\frac{31}{48}f^*_{I-2}+\frac{1}{60}f^*_{I-1}\Big)\,, \quad (24)$$

$$2\Big(\frac{\partial f^*}{\partial z}\Big)_{I-3}+\Big(\frac{\partial f^*}{\partial z}\Big)_{I-2}=\frac{1}{\Delta z}\Big(-\frac{1}{60}f^*_{I-6}+\frac{1}{6}f^*_{I-5}-1f^*_{I-4}-\frac{4}{3}f^*_{I-3}+\frac{25}{12}f^*_{I-2}+\frac{1}{10}f^*_{I-1}\Big)\,. \quad (25)$$

Once $\frac{\partial \boldsymbol{F}^*}{\partial x}$ is known from Eqs. (21) trough (25), the system of equations shown in Eq. (4) can be rewritten as shown in Eq. (26):

$$\frac{\partial \boldsymbol{Q}}{\partial t}=-\frac{\partial \boldsymbol{F}^*}{\partial z}+\boldsymbol{S}=\boldsymbol{G}(\boldsymbol{Q})\,. \quad (26)$$

This form of the Equation can then be integrated in time using a standard fourth order Runge-Kutta method (Lomax *et al.*, 2003) shown in Eq. (27), where Δt is the time step:

$$\begin{aligned}
&\underline{\boldsymbol{Q}}_1=\boldsymbol{Q}^n\\
&\underline{\boldsymbol{Q}}_2=\boldsymbol{Q}^n+\tfrac{1}{2}\Delta t\boldsymbol{G}(\underline{\boldsymbol{Q}}_1)\\
&\underline{\boldsymbol{Q}}_3=\boldsymbol{Q}^n+\tfrac{1}{2}\Delta t\boldsymbol{G}(\underline{\boldsymbol{Q}}_2)\\
&\underline{\boldsymbol{Q}}_4=\boldsymbol{Q}^n+\Delta t\boldsymbol{G}(\underline{\boldsymbol{Q}}_3)\,.
\end{aligned} \quad (27)$$

Note that each sub-step is calculated only after all components of $\boldsymbol{Q}$ have been evaluated for the current step in the Runge-Kutta method. The value of $\boldsymbol{Q}$ at the next time step is then evaluated as shown in Eq. (28):

$$\boldsymbol{Q}^{n+1}=\boldsymbol{Q}^n+\tfrac{1}{6}\Delta t[\boldsymbol{G}(\underline{\boldsymbol{Q}}_1)+2\boldsymbol{G}(\underline{\boldsymbol{Q}}_2)+2\boldsymbol{G}(\underline{\boldsymbol{Q}}_3)+\boldsymbol{G}(\underline{\boldsymbol{Q}}_4)]\,. \quad (28)$$

The eighth-order compact filter (Cook and Cabot, 2005) in Eq. (29) is applied to each component of the conserved variables vector $\boldsymbol{Q}$ after each sub-step of the fourth-order Runge-Kutta method to ensure numerical stability:

$$\beta\hat{q}_{i-2}+\gamma\hat{q}_{i-1}+\hat{q}_i+\gamma\hat{q}_{i+1}+\beta\hat{q}_{i+2}=aq_i+\frac{b}{2}(q_{i+1}+q_{i-1})+\frac{c}{2}(q_{i+2}+q_{i-2})++\frac{d}{2}(q_{i+3}+q_{i-3})+\frac{e}{2}(q_{i+4}+q_{i-4})\,, \quad (29)$$

where $\hat{q}$ is the filtered value of q. Here, q represents any component q_1, q_2 or q_3 of the vector $\boldsymbol{Q}$ defined in Eq. (5). The coefficients γ, β, a, b, c, d and e used in this filter are defined in Eq. (30).

$$\begin{aligned}
&\gamma=0.66624\,, \qquad \beta=0.16688\,, \qquad a=0.99965\,, \qquad \frac{b}{2}=0.66652\,,\\
&\frac{c}{2}=0.16674\,, \qquad \frac{d}{2}=0.16674\,, \qquad \frac{e}{2}=-5\times10^{-6}\,.
\end{aligned} \quad (30)$$

After the Runge-Kutta integration is completed, the vector of conserved variables $\boldsymbol{Q}$ is known at the next time step and the primitive variables can be derived from it. The void fraction α can be expressed in terms of the component q_1 of $\boldsymbol{Q}$:

$$\alpha=\frac{\frac{q_1}{A}-\rho_l}{\rho_l-\rho_g} \quad (31)$$

Substituting this expression into the definition of the component q_3, Eq. (32) is obtained:

$$q_3=\frac{\rho_l A-q_1}{\rho_l-\rho_g}(\rho_g\hat{u}_g-\rho_l\hat{u}_l)+\rho_l\hat{u}_l A \quad (32)$$

The properties are only a function of the saturared state, therefore Eq. (32) determines the flow pressure. The densities ρ_k and internal energies $\hat{u}_k$ of each phase were obtained by polynomial of properties tables from NIST REFPROP (Lemmon *et al.*, 2010). The saturation pressure and temperature are determined solving Eq. (32) using the secant method. Once p is known, ρ_k and $\hat{u}_k$ can be evaluated and the void fraction α is readily available from Eq. (31). The velocities v_k of each phase are obtained from the component q_2 of $\boldsymbol{Q}$ given in Eq. (5) used in conjunction with Eq. (12).

4. RESULTS AND DISCUSSION

Two test cases were employed to verify the proposed numerical method. The first case is a study of a steady-state vertical flow of refrigerant R410a, presented by Barbosa (2017). The case was chosen to validate steady state solution achieved by the present model and also the evaluation of thermophysical properties. The second case is a water-vapor shock tube with interphase mass transfer (Chiapolino *et al.*, 2017), chosen to validate the transient solution of the present model.

4.1 Steady State Vertical R410a flow

A gas-liquid mixture of R410a in the slug regime flows vertically upward through a duct with length $L = 40$ m and diameter $d = 26$ mm. Pressure at the exit of the duct is $p_0 = 1.5$ MPa. The superficial velocities at the inlet at $t = 0$ are set as $j_l = 0.80$ m/s and $j_g = 0.20$ m/s for the liquid and gas phases respectively. From $t = 200$ s to $t = 250$ s, the inlet superficial velocities are smoothly varied, until they reach the final values of $j_l = 0.20$ m/s and $j_g = 0.80$ m/s, which remain constant until the end of the simulation. The drift-flux parameters were evaluated according to a correlation by Bhagwat and Ghajar (2014). The source term s_m for the momentum equation was evaluated according to Eqs. (6). Properties of refrigerant R410a were evaluated by polynomial interpolation from properties tables from NIST REFPROP (Lemmon *et al.*, 2010), except for the viscosities of each phase, which were evaluated according to Geller *et al.* (2000). A computational mesh of $I = 101$ points was used for this simulation.

The model of Barbosa (2017) is a one dimensional steady state model employing a marching procedure. To evaluate phase change, that model assumes a constant mixture enthalpy h_m, defined in Eq. (33):

$$h_m = (1 - x)h_l + xh_g \, , \tag{33}$$

where h_l and h_g are the enthalpies of the liquid and gas phases, respectively, and x is the mixture quality, defined in Eq. (18).

The time history obtained for the mixture enthalpy, h_m, in the present simulation is shown in Fig 1. It can be seen that, from $t = 100$ s to $t = 200$ s the solution is in steady state and the mixture enthalpy is constant throughout the pipe. After $t = 200$ s, due to the change in the inlet conditions, the simulation enters a transient state, reaching a second steady state at approximately $t = 350$ s, when the mixture enthalpy is once again constant in the entire duct. Therefore, in steady state conditions, the mixture enthalpy is constant, in accordance to the results presented by Barbosa (2017).

Results from the first steady state condition are presented in Fig. 2, against the data presented by Barbosa (2017), while results for the second steate condition are shown in Fig. 3. The pressure against pipe length plots, Figs. 2a and 3a, are nearly linear, as most of the pressure gradient comes from the gravitational effect in the vertical flow. The pressure results are within 0.3% of the results from Barbosa (2017). During the first steady state, the void fraction is within 3.5% to the results of Barbosa (2017), while the liquid and gas superficial velocities are within 0.5% and 5.1%, respectively. For the second state, the void fraction and both superficial velocities are all within 1.0% to the reference solution.

The mass flow rates of the gas phase, liquid phase and mixture were also calculated for the two steady state conditions and are shown in Fig. 4. It can be seen that, as the mixture flows upwards inside the duct and pressure falls, the liquid mass flow rate decreases and the gas mass flow rate increases, corresponding to some liquid mass evaporating. However, during steady state conditions, the total mass inside the pipe must remain constant, as can be seen from Eq. (1). During the first steady state, the total evaporated mass between the inlet and outlet is $\dot{m}_{e,1} = 25.3$ g/s, while the total evaporated mass for the second steady state is $\dot{m}_{e,2} = 3.6$ g/s.

4.2 Water-vapor shock tube with phase change

A two-phase shock tube containing water and vapor, proposed by Chiapolino *et al.* (2017) was chosen to validate the transient numerical scheme. The shock tube has a length $L = 1$ m and the discontinuity is set at half of its length, that is, $x_d = 0.5$ m. The homogeneous model was used for this simulation, that is, $v_l = v_g = v$, which can also be expressed by having $C_0 = 1.0$ and $v_d = 0.0$ in Eq. (12). Initial conditions are given in terms of velocity, mixture quality and pressure, with $v = 0$ and $x = 0.2$ in the entire shock tube, $p_L = 0.2$ MPa to the left of the discontinuity and $p_R = 0.1$ MPa to the right of the discontinuity. Thermodynamic properties of saturated water were evaluated using a polynomial interpolation

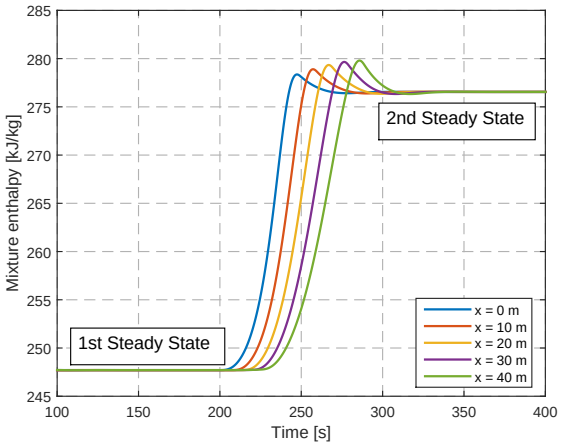

Figure 1: Steady-state solution for the mixture enthalpy.

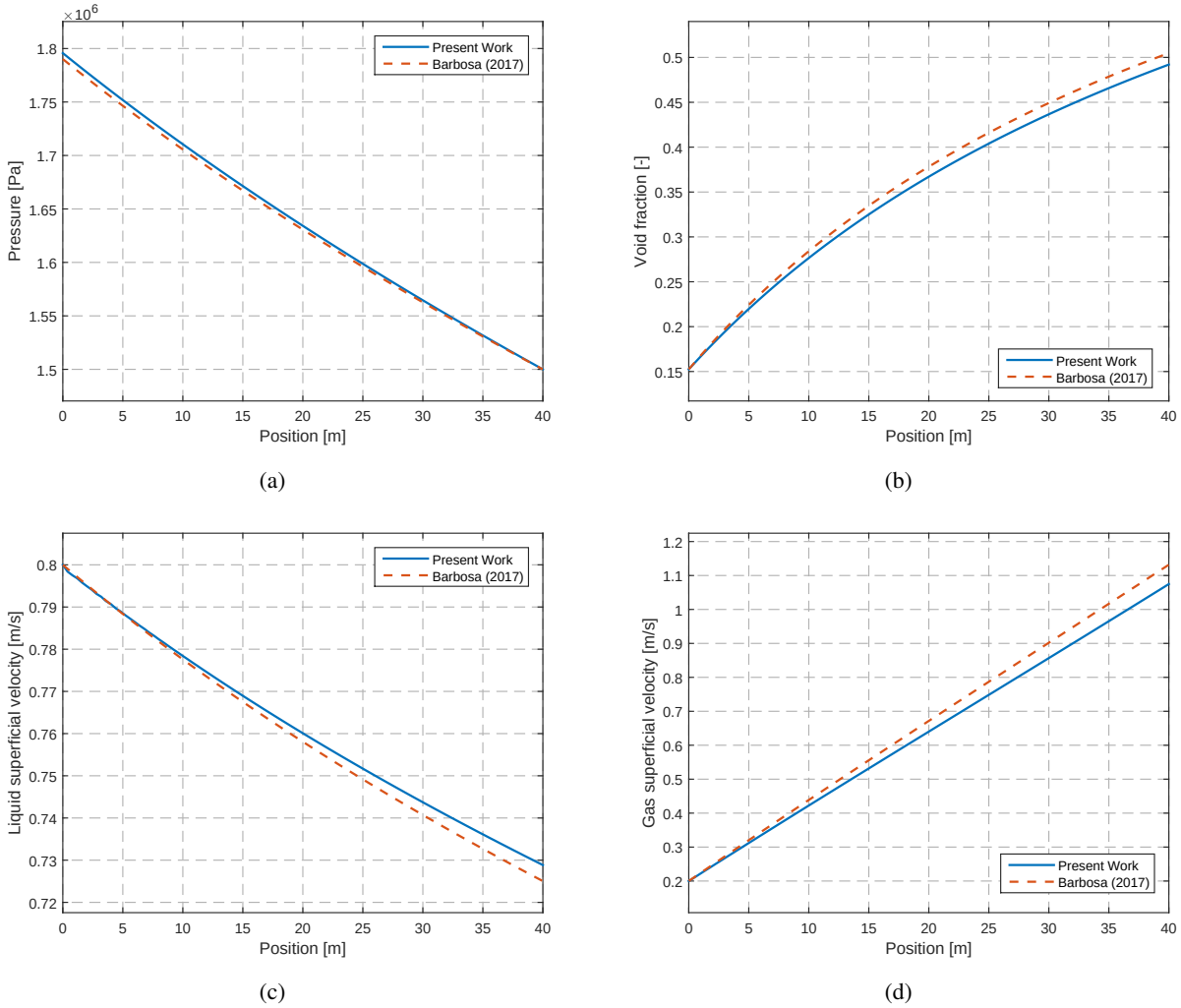

(a) (b) (c) (d)

Figure 2: Comparison of the results obtained in the present work during the first steady state, in blue, and results by Barbosa (2017), in red. Inlet conditions: $j_l = 0.8$ m/s and $j_g = 0.2$ m/s. (a) pressure; (b) void fraction; (c) liquid superficial velocity; (d) gas superficial velocity.

of property tables given by NIST REFPROP (Lemmon *et al.*, 2010). No source terms were considered in this simulation, that is, $s_m = 0$ in Eq. (5). A computational mesh of $I = 101$ discreet points was used for this simulation.

Results are shown in Fig. 5 at time $t = 0.8$ ms. The pressure, mixture density and velocity profiles, shown in Figs. 5a,

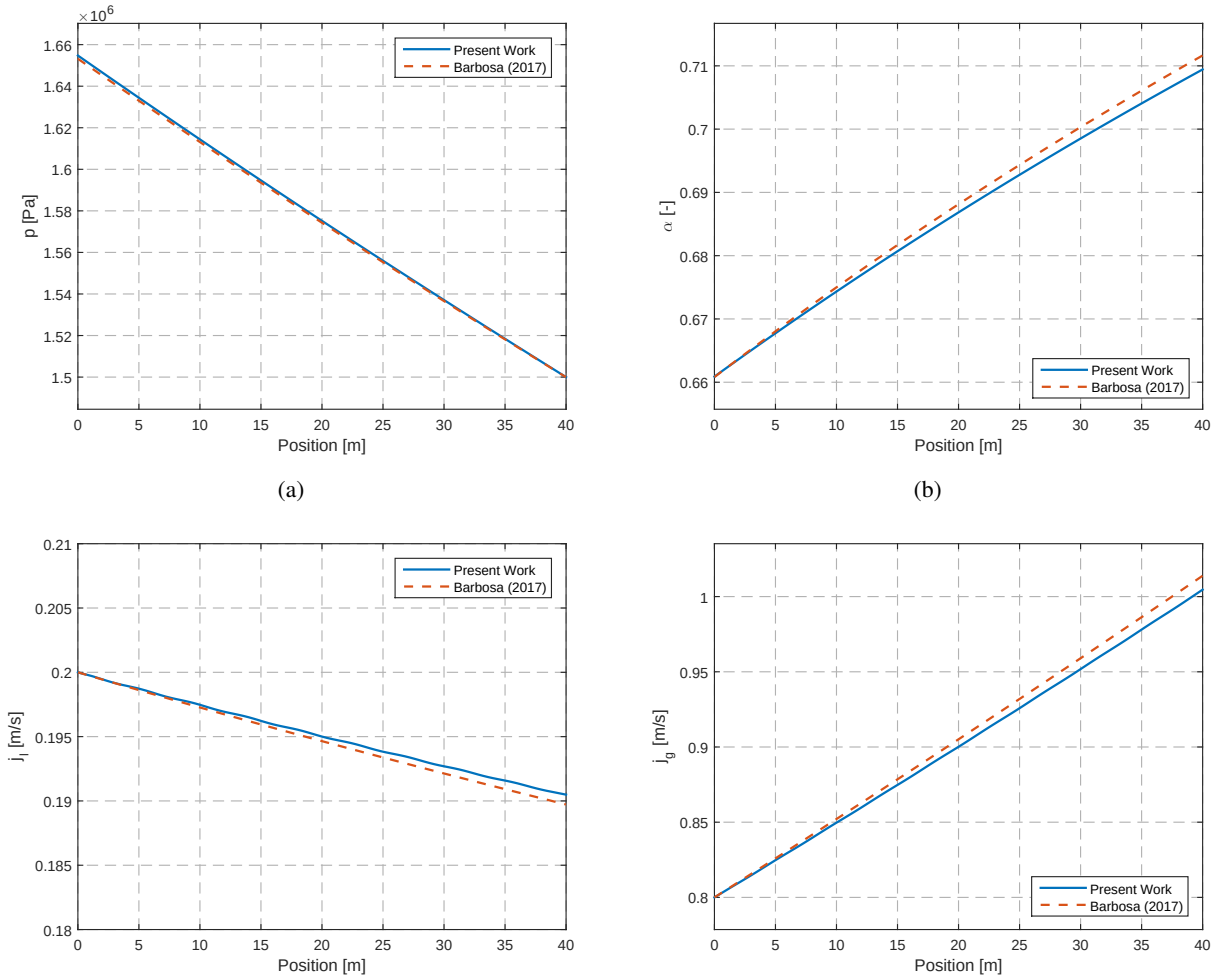

Figure 3: Comparison of the results obtained in the present work during the second steady state, in blue, and results by Barbosa (2017), in red. Inlet conditions: $j_l = 0.2$ m/s and $j_g = 0.8$ m/s. (a) pressure; (b) void fraction; (c) liquid superficial velocity; (d) gas superficial velocity.

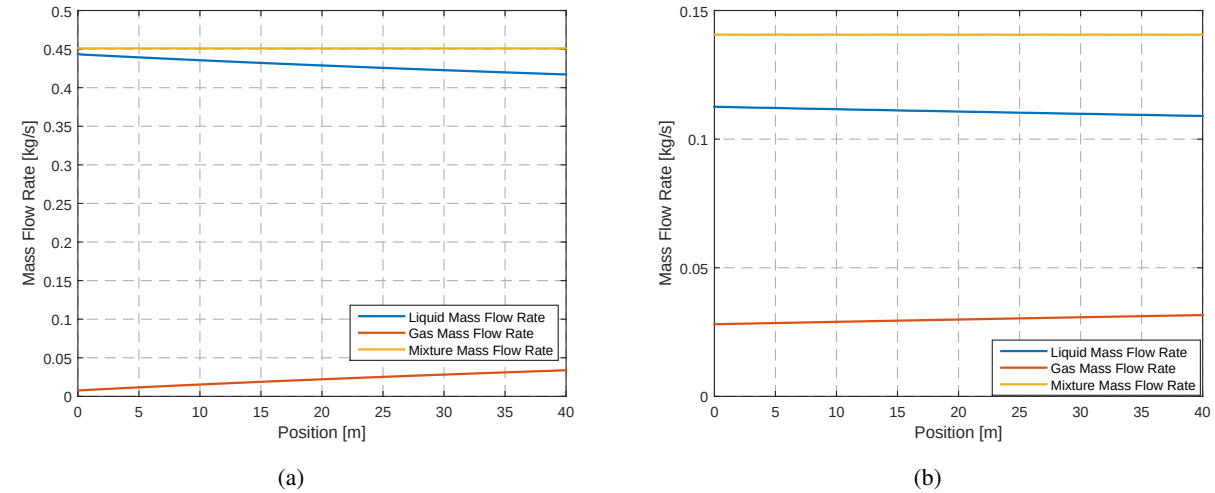

Figure 4: Mass flow rates for the liquid phase (blue), gas phase (red) and mixture (yellow) inside the duct. (a) first steady state condition; (b) second steady state condition

5b and 5c respectively, are in agreement with the reference solution by Chiapolino *et al.* (2017). The present numerical solver is able to capture the discontinuities more sharply than the reference solution. This is due to the present model using an eight-order numerical method, while the reference solution used a first-order Godunov solver. The temperature against pipe length plot, Fig. 5d is also in good agreement with the reference solution. The temperature behavior is well-captured and discontinuities are also captured sharply by the present simulator, as was the case with the previous properties. Temperature values are underestimated by approximately 1 K in the whole domain, compared to the reference solution, a difference that likely arises due to differences in properties evaluation. A similar trend is shown in the profiles of the liquid mass and volume fractions, shown in Figs. 5e and 5f. Both profiles are also in good agreement with the reference solution, but underestimate the reference values due to differences in properties evaluation. The present simulator underestimated the liquid mass fraction by up to 2% and the liquid volume fraction by up 6% when compared to the reference solution.

5. CONCLUSIONS

An eighth-order finite differences compact scheme was assembled to solve transient two-phase flow problems of a saturated pure substance using the drift-flux model. The compact scheme is initially validated against a steady state case from the literature with very good results. The first case was a vertical R410a flow, where mixture enthalpy in steady state conditions was approximately constant and the pressure solution was within 0.3% of the reference results, while the void fraction and superficial velocities were within 5.1% of the reference solution. The present simulator was also validated against a shock-tube solution from the literature, showing its capabilities to capture sharp discontinuities in the numerical solution. The next developments on the model concern the introduction of a model to handle non-equilibrium flow and also the transition from a single phase flow of liquid or gas into two-phase flow.

6. ACKNOWLEDGEMENTS

Bruno Resende Rodrigues acknowledges CAPES for his doctoral scholarship.

7. REFERENCES

Barbosa, M.R., 2017. *Estudo da Influência da Densidade do Gás no Escoamento Bifásico Gás-Líquido Usando um Modelo de Mistura*. Phd thesis, Faculty of Mechanical Engineering, State University of Campinas.

Beattie, D.R.H. and Whalley, P.B., 1982. "A simple two-phase frictional pressure drop calculation method". *Int. J. Multiph. Flow*, Vol. 8, No. 1, pp. 83–87.

Bhagwat, S.M. and Ghajar, A.J., 2014. "International Journal of Multiphase Flow A flow pattern independent drift flux model based void fraction correlation for a wide range of gas – liquid two phase flow". *Int. J. Multiph. Flow*, Vol. 59, pp. 186–205. ISSN 0301-9322.

Brown, S., Martynov, S., Mahgerefteh, H. and Proust, C., 2013. "International Journal of Greenhouse Gas Control A homogeneous relaxation flow model for the full bore rupture of dense phase CO 2 pipelines". *Int. J. Greenh. Gas Control*, Vol. 17, pp. 349–356. ISSN 1750-5836.

Chiapolino, A., Boivin, P., Saurel, R., Chiapolino, A., Boivin, P. and Saurel, R., 2017. "A simple phase transition relaxation solver for liquid-vapor flows". *Int. J. Numer. Methods Fluids*, Vol. 83, No. 7, pp. 586–605.

Cook, A.W. and Cabot, W.H., 2004. "A high-wavenumber viscosity for high-resolution numerical methods". *J. Comput. Phys.*, Vol. 195, pp. 594–601.

Cook, A.W. and Cabot, W.H., 2005. "Hyperviscosity for shock-turbulence interactions". *J. Comput. Phys.*, Vol. 203, pp. 379–385.

Downar-Zapolski, P., Billick, Z., Bolle, L. and Franco, J., 1996. "The non-equilibrum relaxation model for one-dimensional flashing fliquid flow". *Int. J. Multiph. Flow*, Vol. 22, No. 3, pp. 473–483.

Geller, V.Z., Bivens, D. and Yokozeki, A., 2000. "Viscosity of Mixed Refrigerants , R404A , R407C ,". *Int. Refrig. Air Cond.*, Vol. 8, pp. 399–406.

Lele, S.K., 1992. "Compact Finite Difference Schemes with Spectral-like Resolution". *J. Comput. Phys.*, , No. 103, pp. 16–42.

Lemmon, E.W., Huber, M.L. and McLinden, M.O., 2010. *NIST Standard Reference Database 23: Reference Fluid Thermodynamic and Transport Properties - REFPROP*. National Institute of Standards and Technology, Standard Reference Data Program, Gaithersburg, 9th edition.

Leveque, R.J., 2002. *Finite volume methods for hyperbolic equations*. Cambridge University Press.

Lomax, H., Pulliam, T.H. and Zingg, D.W., 2003. *Fundamentals of Computational Fluid Dynamics*.

Lorenzo, M.D., Lafon, P., Matteo, M.D., Pelanti, M., Seynhaeve, J. and Bartosiewicz, Y., 2017. "Homogeneous two-phase flow models and accurate steam-water table look-up method for fast transient simulations". *Int. J. Multiph. Flow*, Vol. 95, pp. 199–219. ISSN 0301-9322.

Lund, H. and Aursand, P., 2012. "Two-Phase Flow of CO 2 with Phase Transfer". *Energy Procedia*, Vol. 23, pp. 246–255.

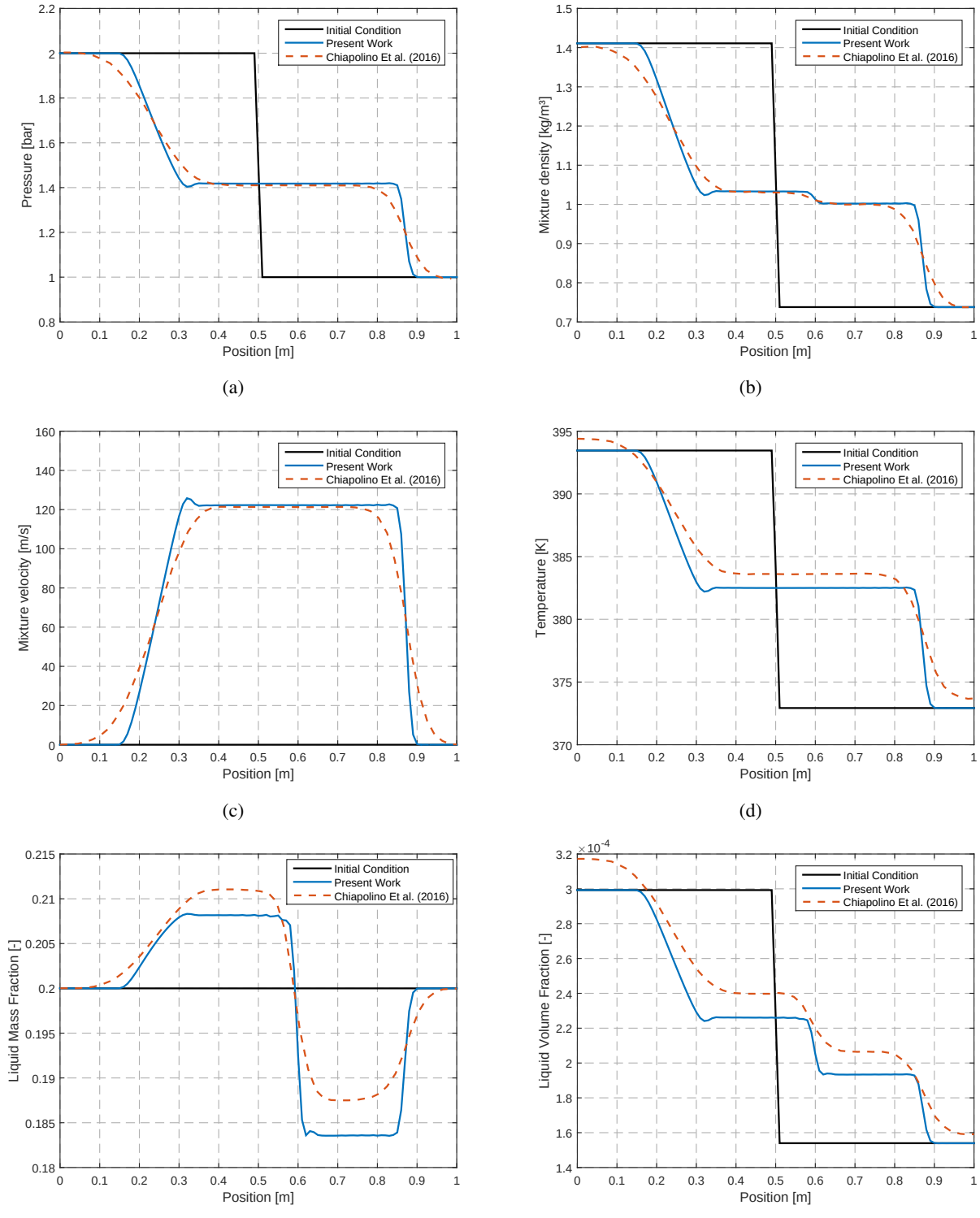

Figure 5: Comparison of the results obtained in the present work, in blue, and results by Chiapolino *et al.* (2017), in red for the shock tube problem at $t = 0.8$ ms. (a) pressure; (b) mixture density; (c) mixture velocity; (d) temperature; (e) liquid mass fraction and (f) liquid volume fraction.

ISSN 1876-6102.

Saurel, R., Petitpas, F. and Abgrall, R., 2008. "Modelling phase transition in metastable liquids: Application to cavitating and flashing flows". *J. Fluid Mech.*, Vol. 607, pp. 313–350.

Toro, E.F., 2009. *Riemann solvers and numerical methods for fluid dynamics*. Springer.

Zuber, N. and Findlay, J.A., 1965. "Average Volumetric Concentration in Two-Phase Flow Systems". *J. Heat Transfer*, Vol. 87, No. 4, pp. 453–468.

8. RESPONSIBILITY NOTICE

The authors are the only responsible for the printed material included in this paper.